Acid-induced demineralisation of human enamel as a function of time and pH observed using X-ray and polarised light imaging

Harper, Robert; Shelton, Richard; James, Jonathan; Salvati, Enrico; Besnard, Cyril; Korsunsky, Alexander M.; Landini, Gabriel

DOI:
10.1016/j.actbio.2020.04.045

Acid-induced demineralisation of human enamel as a function of time and pH observed using X-ray and polarised light imaging

Robert A. Harper[1*], Richard M. Shelton[1], Jonathan D. James[1], Enrico Salvati[2], Cyril Besnard[2], Alexander M. Korsunsky[2], and Gabriel Landini[1]

[1] School of Dentistry, Institute of Clinical Sciences, University of Birmingham, 5 Mill Pool Way, Edgbaston, Birmingham, B5 7EG, UK

[2] Department of Engineering Science, University of Oxford, Parks Road, Oxford, OX1 3PJ, UK

[*]**Corresponding author:** Dr Robert A. Harper. University of Birmingham, School of Dentistry, 5 Mill Pool Way, Edgbaston, Birmingham, B5 7EG. E-mail: r.a.harper@bham.ac.uk.

Abstract

Acid-induced enamel demineralisation affects many individuals either by exposure to acidic diets, acidic gas pollution (dental erosion) or to dental plaque acids (dental caries). This study aimed to develop *in situ* X-ray and light imaging methods to determine progression of enamel demineralisation and the dynamic relationship between acid pH and mineral density.

Hourly digital microradiograph time-lapse sequences showed the depth of enamel demineralisation in 500 µm thick sections progressed with time from the surface towards the dentine following a power-law function, which was 21% faster than the lateral demineralisation progression after exposure for 85 h to lactic acid (10%, pH 2.2). The minimum greyscale remaining (mineral content) within the induced enamel lesion followed an exponential decay, while the accumulated total greyscale loss with time was linear, which showed a constant anisotropic mineral release within the enamel architecture. This 85h demineralisation method studied by polarised light microscopy time-lapse sequences showed that once the demineralisation front reached the enamel Hunter-Schreger bands, there was preferential demineralisation along those bands.

Mineral density loss was linear with increasing pH acidity between pH 5.2 and pH 4.0 (with 0.4 pH increments) when incubated over a 3-week period exposed to 0.5% lactic acid. At pH 4.0, there was complete mineral loss in the centre of the demineralised area after the 3-week period and the linear function intercepted the x-axis at ~ pH 5.5, near the critical pH for hydroxyapatite (HAp). These observations showed how intrinsic enamel structure and pH affected the progression of demineralisation.

Keywords: Enamel; demineralisation; imaging; *in situ*; kinetics.

1. Introduction

Dental caries is the most prevalent disease in modern humans [1], [2], [3] and considerable efforts are made to promote good oral hygiene by routine mechanical removal of plaque (brushing with dentifrices), use of antimicrobial and fluoridated agents and the avoidance of a high sugar diet [4]. However, the high prevalence of the disease indicates that current methods and products are not able to completely prevent it. This paper examines the possible role of intrinsic enamel structure factors and pH in dental caries progression in order to gain understanding of the dynamics of the demineralisation process and aid in the development of improved prevention, diagnosis and restorative treatments [5], [6], [7]. Theoretical mathematical models of caries initial propagation and progression have been proposed but still require experimental validation [8], [9].

Enamel, the outer most layer of teeth, is the hardest tissue in the human body, consisting of 96% hydroxyapatite ($Ca_{10}(PO_4)_6(OH)_2$) (HAp), 3% water and 1% organic material [10]. Enamel demineralisation is initiated by exposure to acidic conditions, causing hydroxyapatite dissolution. Whilst the critical pH at which this occurs depends on a variety of factors, it is generally accepted to be around pH 5.5 [11]. Dental caries is associated with acidogenic bacteria forming sticky biofilms that rapidly metabolise carbohydrates and excrete acids *e.g.* lactic acid [12]. The microbiological element of dental caries is fundamental to the disease, but there are numerous variables, which can affect cariogenicity *e.g.* bacterial species, biofilm composition, saliva composition, as well as quantity, type and frequency of carbohydrate intake in diet. Since this study aimed to characterise the process of acid demineralisation of enamel, an acid-only caries model was used.

Bulk enamel has a prismatic structure consisting of 5 μm sized HAp rods (with a small amount of organic material remaining after enamel mineralisation and maturation

processes) containing crystallites orientated with long axes that run parallel to the longitudinal axis of the rod and HAp inter-rods which contain crystallites that laterally flare until orientated approximately perpendicular to the rods [13]. Acid-induced enamel demineralisation has shown preferential rod dissolution patterns (type 1), preferential inter-rod dissolution (type 2) and a mixture of both (type 3) when imaged using scanning electron microscopy (SEM) [14], [15]. This anisotropic HAp dissolution has also been observed in small and wide angle X-ray scattering synchrotron experiments [16]. The demineralisation pattern in enamel caries is initially type 2 but as lesions deepen type 1 demineralisation becomes more prevalent [17]. However, SEM observations have focused on *ex-situ* prism scale changes and have not taken into account *in situ* kinetics or the schmelzmuster anisotropy, *e.g.* radial enamel (parallel prism arrangement) and Hunter-Schreger bands (HSBs) (bundles of parallel prisms with alternating tilt angles (decussating)) [18], [19], which could affect the kinetics of acid front advance.

Radiographic longitudinal studies of human enamel demineralisation has the potential to overcome these issues [20] but has not yet harnessed the digital microradiographic imaging capability of microcomputed tomography (micro-CT) equipment which can be used for automated *in situ* 2D imaging, enabling more time points to be captured with high image resolution. Light microscopy imaging of longitudinal tooth sections can also detect enamel demineralisation. Early stage carious lesions in enamel (without cavitation), are typically organised into four or five zones according to refraction patterns of light. From the tooth surface towards the depth of the enamel these zones are referred to as the surface zone, the body of the lesion, the dark zone and translucent zone. An extra translucent zone is sometimes seen between the dark zone and the body of the lesion. All of these zones are thought to represent changes in enamel porosity and crystallite content [21] that result in altered and localised refraction properties of enamel. However, this technique has not been

fully utilised to image the demineralisation process *in situ* nor been compared with an *in-situ* digital microradiography technique.

To fully characterise the demineralisation process other factors need attention, including the pH of the environment in contact with enamel. It is well established that as pH decreases, the severity of enamel demineralisation increases [22] but the relation between the two has not been precisely established to date. Therefore, the aim of this work was to assess enamel demineralisation as a function of time and pH as well as elucidating how demineralisation related to the intrinsic properties of enamel. Automated time-lapse experiments were established to monitor the *in situ* enamel demineralisation by lactic acid, using digital microradiography and polarised transmitted light microscopy (PTLM) to determine the kinetics of the demineralisation advance. Comparison between demineralisation detected by digital microradiography and PTLM was made to establish any differences in sensitivity of the two techniques. The mineral density change in relation to lactic acid pH as well as assessing the shape of demineralised lesions that resulted was established using micro-CT 3D reconstructions.

2. Materials & Methods

2.1 Sample preparation

The study used intact human third molars extracted for non-caries related therapeutic reasons (National Research Ethics Committee; NHS-REC reference 09.H0405.33/ Consortium Reference BCHCDent332.1531.TB). Tooth root tips were removed using a low speed rotating diamond saw (Isomet, UK) before sterilisation in 10% formalin buffered solution (Sigma Aldrich, UK) for four days. Teeth were then rinsed with water and sectioned into 500 µm thick slices from the buccal to the lingual surfaces, the slices were then cut in half separating the buccal and lingual surfaces. Each non-carious slice had a flat tipped 300

μm diameter needle (Septodont, France) clamped perpendicularly on the external enamel surface before coating the surface with commercially available nail varnish. The buccal/ lingual enamel was selected as these areas provided multiple samples containing the best distinction between radial and decussating enamel to detect the schmelzmuster level demineralisation *e.g.* occlusal enamel contains rods that often change direction, which could have made the distinction more difficult to observe. Removal of the needle left an ~ 300 μm diameter circular non-varnished area on the slice (Figure 1). Twenty-five of these 500 μm thick-varnished slices were prepared from ten non-carious teeth; four slices (one per tooth) for the time-lapse digital microradiography, three slices (one per tooth) for the time-lapse PTLM and eighteen slices (six per tooth) for the pH micro-CT study. In addition, three 500 μm thick slices from three carious teeth (one per tooth), containing non-cavitated smooth surface carious lesions were prepared. All samples were stored in phosphate-buffered saline (PBS) prior to use.

2.2 Sample demineralisation as a function of time

Tooth slices for *in situ* digital microradiograph imaging were placed in a radiolucent Kapton® sheet (DuPont™, USA) holder (made with 5 x 4.5 cm pieces) (see supplementary material, Figure A1). Three gutta-percha points (size 40) were glued with cyanoacrylate between the Kapton® sheets (one per edge) to act as spacers to provide a volume for an acid chamber and seal the margins. Lactic acid (10 % v/v, 0.5 mL, pH 2.2) was injected into the opening of the Kapton® holder to induce enamel demineralisation and simulate an accelerated caries process [23]. Finally, the opening of the sample holder was sealed using molten dental ribbon wax to prevent the evaporation of the acid. Samples were then time-lapse imaged into digitally microradiograph using a SkyScan 1172 micro-CT scanner (Bruker, Belgium) at 60 kV and 167 μA in the presence of a 0.5mm aluminium filter at ambient temperature (22°C), using 12 times frame averaging (for noise reduction). The

sample stage was positioned to provide images containing inter-pixel distances of 3.02 μm (~ 6 x 4 mm field of view) in all frames as calculated by the instruments internal pixel size calibration. This value was found to have a sampling error below 2% following imaging stainless steel ball bearings of known diameters (0.3 mm, 0.5 ± 0.006 mm 0.9 ± 0.002 mm and 1.5 ± 0.002 mm) (Bearing Warehouse Ltd, UK). Time-lapse sequence were captured using multiple frames captured at intervals of 1 h (in total 86 frames). This was time-lapse sequence digital microradiography not time-lapse sequence micro-CT as there was no rotation between frames. Greyscale (mineral content) profiles over time were generated by sampling the digital microradiographs (linear scan) from the enamel free surface edge through the enamel and dentine using a similar methodology to Deblem et al [24]. The distance from the enamel surface to the point where the readings reached a plateau (*i.e.* intact enamel), were used to calculate the demineralisation front advance. The plateau values were identified by fitting a line through the intact enamel part of the scan lines and selecting the first point of the scan line that intercepted the intact enamel fitted line. Similarly, the width of the demineralised lesion was measured by linearly scanning across the subsurface enamel immediately beneath the acid exposure area and measuring the distance between two plateaus (*i.e.* apparently intact enamel). Greyscale values within the demineralised areas were collected using ImageJ's freehand selection tool by selecting the 85h lesion on each individual digital microradiograph to identify changes in the greyscale with time.

Tooth slices for light microscopy *in situ* imaging were glued with cyanoacrylate to the base of a petri dish (35 x 10mm), to which 5ml of lactic acid (10 % v/v, pH 2.2) was added before securing the petri dish lid with Parafilm™ (to prevent acid evaporation). Samples were then time-lapse imaged (every 100 seconds) using a polarised light microscope (Zeiss Primotech D/A POL, UK) with a 5x objective. The digital microradiography and PTLM experiments were repeated to N = 4 and N = 3 respectively. The pH was checked after each

experiment and remained unchanged. At the end of the *in situ* experiments, samples were placed in PBS (pH 7.4) for 24 h to ensure quenching of the demineralisation process and then imaged using digital microradiography and PTLM for comparison.

2.3 Enamel demineralisation as a function of pH

Varnished tooth slices were incubated at 37°C in lactic acid (0.5% v/v, 0.5mL) (to simulate the carious process [23]) for three weeks at pH 3.6, 4.0, 4.4, 4.8 and 5.2 whilst deionised water (DW) was used as a control with pH 7.0 (one tooth provided six slices, one slice per pH, repeated to N = 3). Solutions were changed every two days to ensure the acidic environment was maintained. The samples were then imaged using the micro-CT method described previously (3.02 μm voxels) except the rotation step was 0.45° with four averaging frames to enable reconstructions as the samples were measured *ex situ* and therefore were micro-CT reconstructions and not digital microradiographs. At the demineralised locations, each sample stayed entirely within the field of view (~ 6 x 4 mm) at each rotation step (no partial volumes). The micro-CT data was reconstructed into Z-stacks using SkyScan's NRecon software (using optimised settings determined qualitatively: smoothing 10, ring artefacts reduction 16, beam hardening 20%, adjusting output maximum 0.2, auto adjusted output minimum) and rendered using ImageJ's Volume Viewer plug-in [25]. The reconstructions were stored in TIFF format and analysed to determine the lesions' depth, width and minimum grey scale values as described earlier. The mineral content of the reconstructions was calibrated to mineral density using six in house made HAp phantom discs. The six HAp discs had densities of 2.76, 2.64, 1.79, 1.67, 1.53 and 0.93 g/cm^3 and were made by pressing HAp powder (Sigma Aldrich, UK) in a mould in an engineering vice. The differences in mineral density were achieved by sintering at 800°C, 900°C, 1000°C, 1100°C and 1250°C for 2h (the lowest mineral density phantom was not sintered) to produce the phantom discs 7.4-9.5 mm in diameter and 1-2 mm in thickness. These discs were then glued

together using cyanoacrylate and polished to approximately half their original diameters in order to entirely fit in the micro-CT field of view (see supplementary material, Figure A2). Greyscale measurements were taken from the reconstructed Z-stack data and measuring the background greyscale provided a 0.00 g/cm^3 data point. Volumes of the discs were determined by reconstructing the Z-stacks, thresholding the images, then multiplying the total number of white pixels by the voxel/ micron ratio. N.B. this mineral density calibration set was used to quantify mineral density for micro-CT experiments (pH variation) only and not the digital microradiography experiments (time-lapse sequences) as the calibration discs were not the same dimensions as the samples.

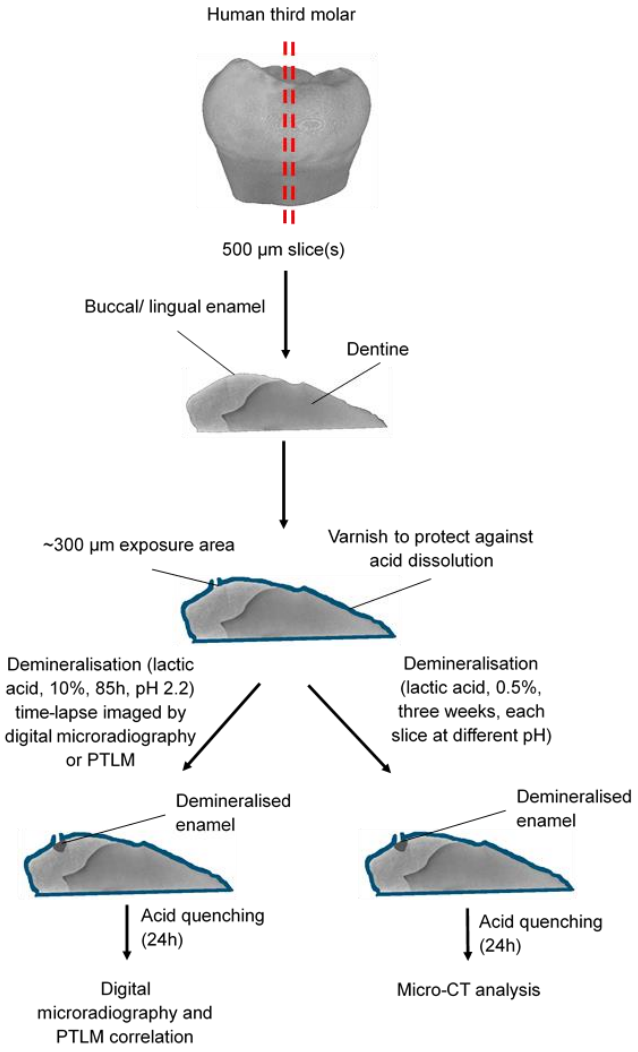

Figure 1: Schematic diagram depicting processes for sample preparation.

2.4 Data analysis

Data were plotted in Sigma Plot version 13.0 (Systat Software Inc, San Jose, California, USA) and statistical analysis used the Shapiro-Wilk's test for normality and one-way ANOVA with Dunn's test for multiple comparisons.

3. Results

Micro-CT images generated from the *in situ* experiments were compiled into temporal stacks to visualise enamel demineralisation progression with time (Figure 2). Enamel demineralisation occurred almost instantly but did not progress linearly. Certain enamel regions appeared to be more acid-resistant than others, most notably at the surface. In addition, the demineralisation advance front was not always smooth or rounded, suggesting that preferential demineralisation was dependent on the structural anisotropy of enamel.

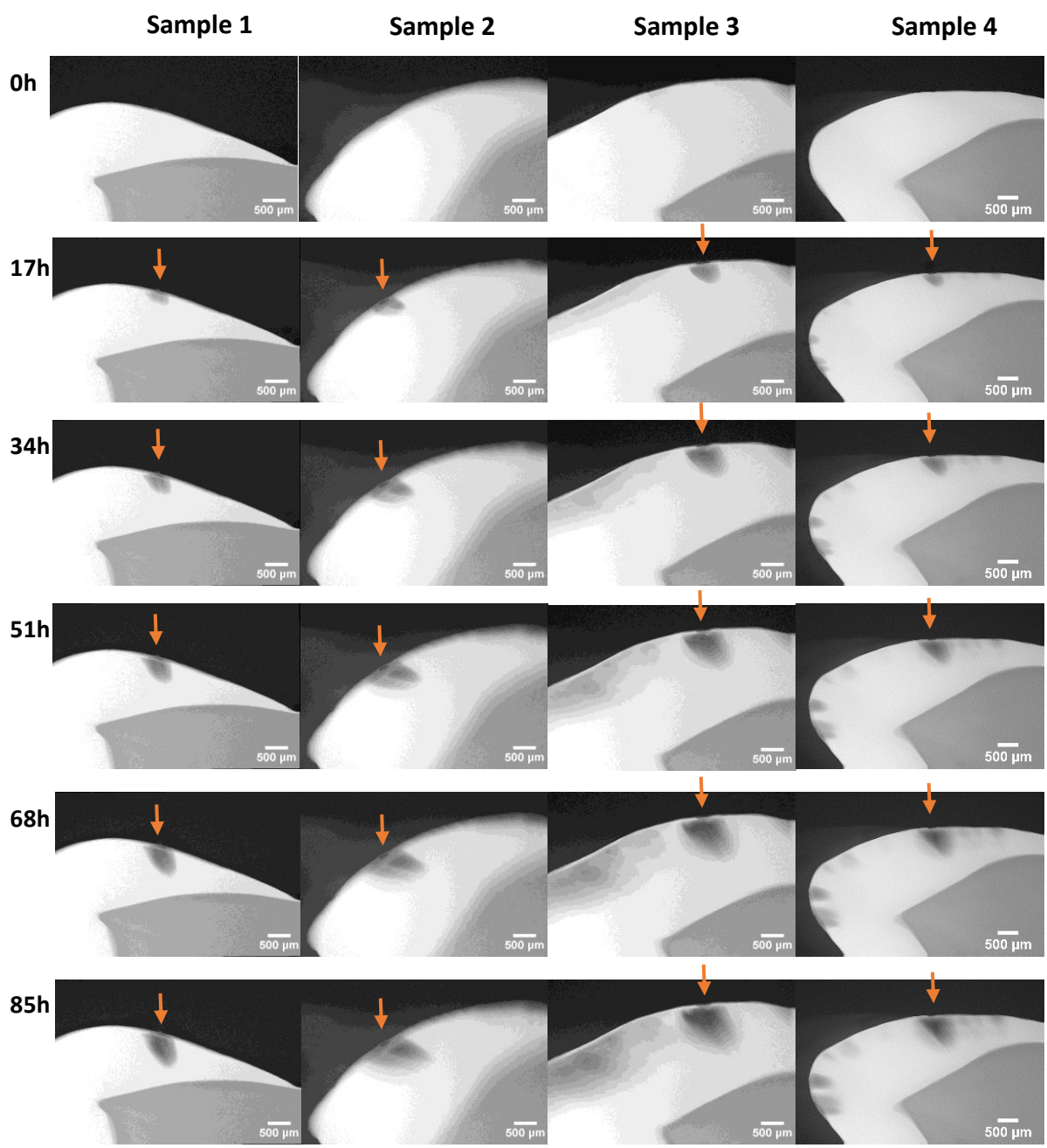

Figure 2: Digital microradiography images from time-lapse sequences showing the evolving demineralisation caused by lactic acid (10% v/v, pH 2.2) in 17h steps. N.B. orange arrows denote intended demineralisation locations, other areas of demineralisation were due to incomplete varnish protection. Each sample was prepared from a separate tooth.

The demineralisation front kinetics were investigated by monitoring greyscale data profile lines at 1h intervals (85 hours in total) for the four samples running from the enamel

free surface to the dentine (demineralised enamel depth) and across the immediate subsurface enamel (demineralised enamel width), on each time frame (see supplementary material, Figure A3). This enabled calculation of the speed the demineralisation front depth advanced (figure 3A). The data was found to fit with a power-law function ($y = ax^b$, a = 77.93, b = 0.59, $R^2 = 0.99$). The maximum depth of enamel demineralisation after 85h of exposure was 1042 ± 198 µm at pH 2.2, 0.5 ml and at ambient (22°C) temperature. Measuring the distance across the immediate subsurface enamel on every frame enabled calculation of the speed of demineralisation front width advance (Figure 3B) which also followed a power-law function ($y = ax^b$, a = 262.05, b = 0.34, $R^2 = 0.97$). Interestingly the b constants in these equations showed the advance in depth of the demineralisation front was faster than the advance in width, indicating a preferential path of demineralisation. In addition, the minimum greyscale (mineral content) in the demineralised enamel areas (Figure 3C) followed an exponential decay function ($y = a * e^{b/(x+c)}$, a = 5602.50, b = 55.17, c = 47.04, $R^2 = 0.99$) with 42% remaining mineral content in the most severely demineralised areas after 85h acid exposure. However, the total rate of greyscale loss from the enamel (figure 3D) was linear ($y = y_0 + ax$, $y_0 = -0.60$, a = 0.34, $R^2 = 0.99$) which indicated a continuous but anisotropic demineralisation.

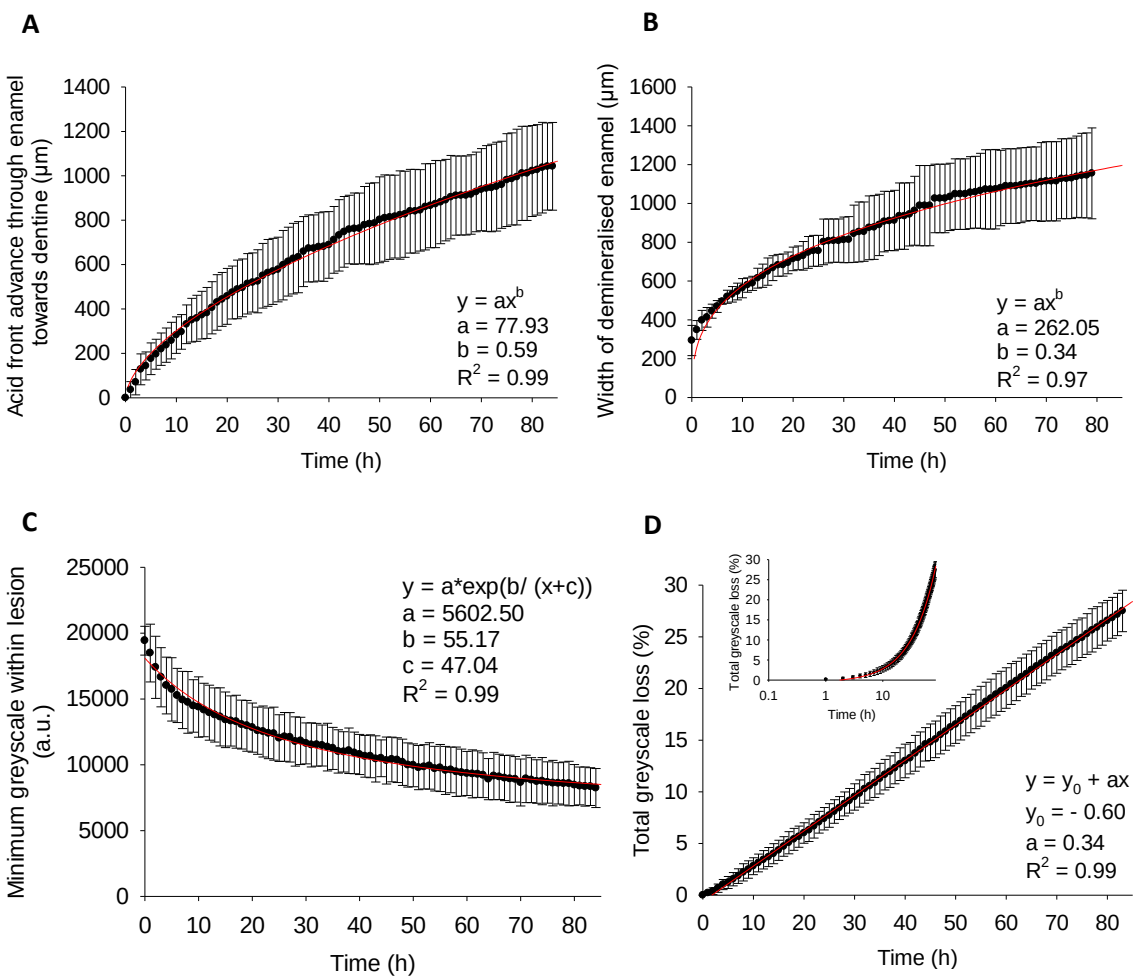

Figure 3: Using lactic acid (10% v/v, pH 2.2), the progression of the demineralisation front depth (A) and width (B) followed power-law processes. The minimum mineral density remaining within lesions demonstrated an exponential decay model (C), whilst the rate of total mineral loss (D) was linear showing that a type of mineral environment within prismatic enamel structure was preferentially demineralised at a constant rate (data presented show mean ± standard deviation). Note the lag time during the first few hours (D) and hence negative y-intercept, showed an initial inhibition of mineral release, the log plot inset highlights this.

Light microscopy time-lapse sequences showed that as the demineralisation advanced, the front appeared to follow HSBs (~ 100 µm wide) preferentially and determine the shape of the lesions (Figure 4).

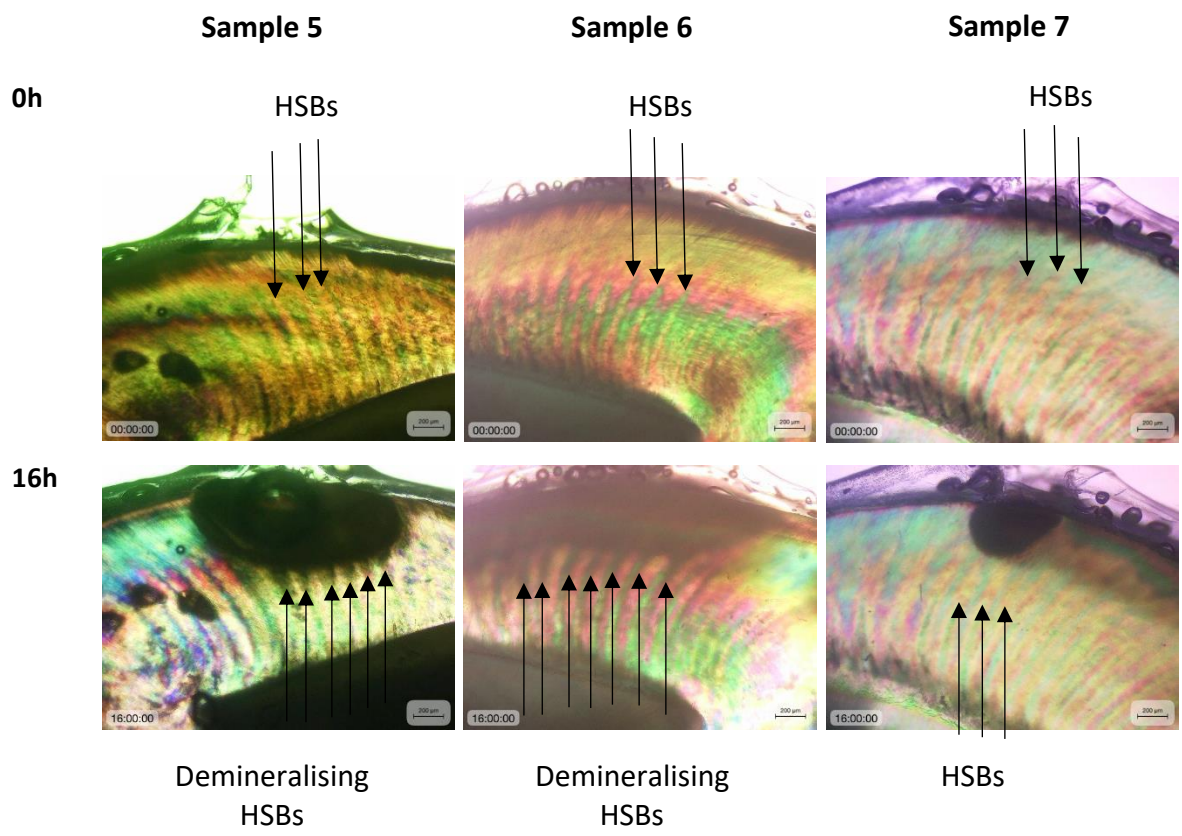

Figure 4: Polarised transmitted light microscopy time stamped image sequence showing the demineralisation characteristics of enamel in the presence of lactic acid (10% v/v, pH 2.2). Intact enamel at 0h and after 16h acid exposure. Gas bubbles appearing during the experiment were likely be carbon dioxide generated from carbonated hydroxyapatite dissolution in excess acid ($CO_3^{2-} + 2H^+ \rightarrow CO_2 + H_2O$). Each sample was prepared from a separate tooth.

Comparing some digital microradiograph and PTLM images of acid quenched samples showed the demineralised areas were larger in PTLM, which indicated that some degree of enamel demineralisation was not detected by X-rays (Figure 5).

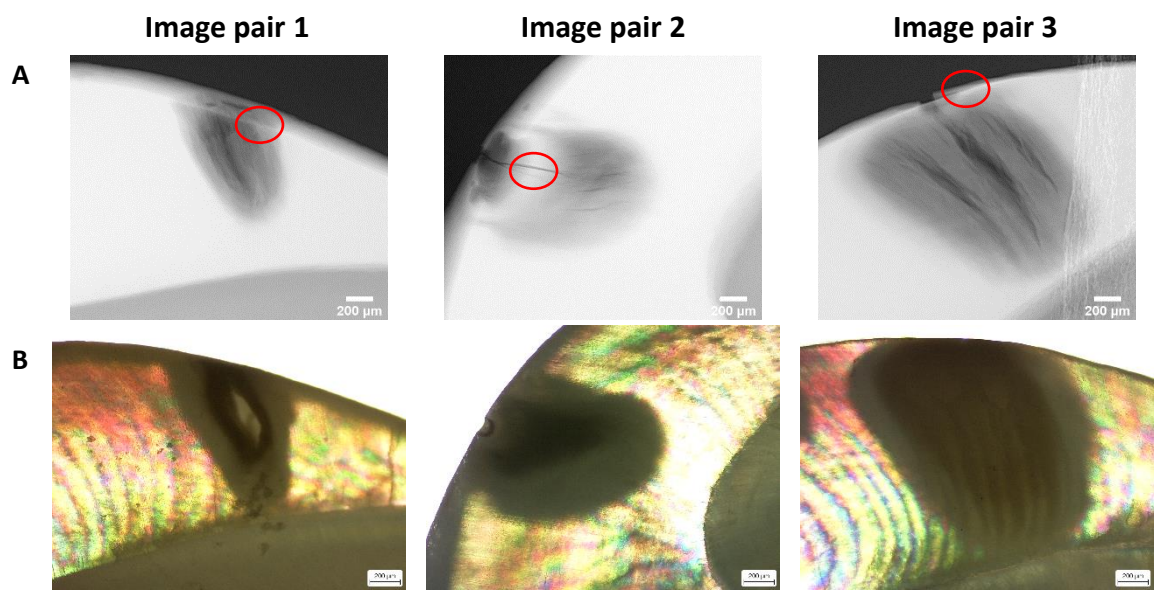

Figure 5: *Ex situ* comparison of induced enamel demineralisation detection *via* digital microradiography (A) and polarised transmitted light microscopy (B) showing that the same sample demineralisation areas were larger in light images than X-ray images (more sensitive to light detection) *i.e.* in image pairs 1 and 3, the demineralised areas reached the DEJ whereas in the digital microradiographs they had not. Surface zones are highlighted with a red circle in the digital microradiographs.

Further analysis performed on natural white spot lesions confirmed this, as lesions were clearly visible using PTLM but not detectable with digital microradiography imaging (See supplementary material, Figure A4). The effect of pH on enamel (Figure 6) resulted in larger and more radiolucent lesions with lower pH values and a less radiolucent zone (~ 30 µm thick) remained visible at the surface of most lesions even at the lowest pH [26].

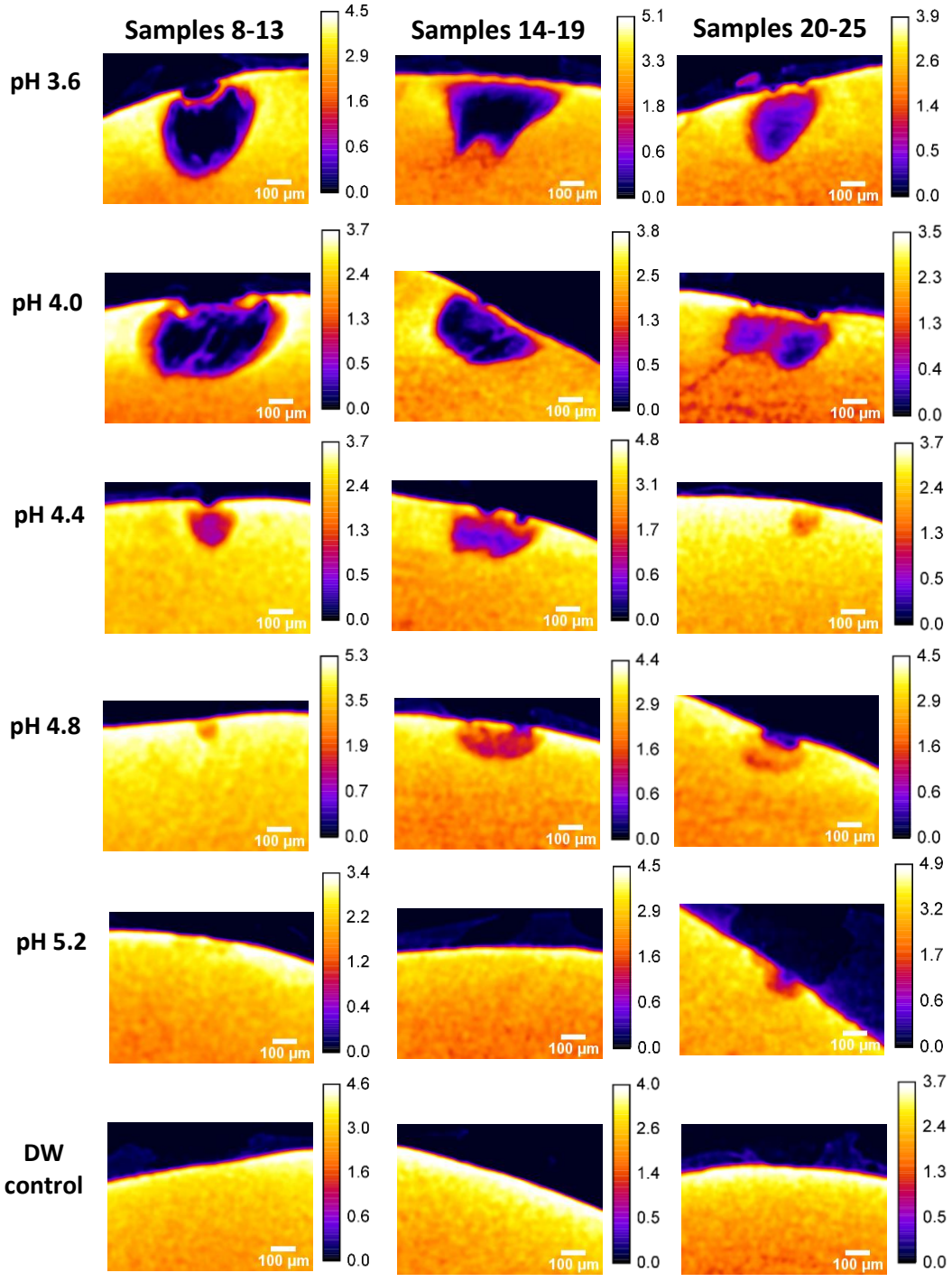

Figure 6: *Ex situ* micro-CT 3D reconstructions, orientated perpendicular to slices in ImageJ volume viewer (and images cropped), of demineralised enamel generated with lactic acid (0.5% v/v) at a range of pH values after 3 weeks incubation with mineral density calibration bars inset (g/cm^3). N.B. Edge effect beam hardening at some sample peripheries generated

375 artificially high mineral density values *i.e.* values above ~ 3.2 g/cm^3. Each column are six
376 samples prepared from the same tooth.

377 Demineralised enamel depth as a function of pH increased as the environment became
378 more acidic linearly ($y = y_0 + ax$, $y_0 = 954.85$, $a = -174.67$, $R^2 = 0.95$) (Figure 7A) and had an
379 x-axis intercept near pH 5.5. The same trend was observed in the demineralised enamel width
380 but the linear function fitted less well ($y = y_0 + ax$, $y_0 = 1276.40$, $a = -214.80$, $R^2 = 0.77$)
381 (Figure 7B) and there was not an x-axis intercept near pH 5.5. This was not surprising, as
382 demineralisation progression laterally across prismatic enamel (permeation across rods, inter-
383 rods and organic sheafs) would be expected to be different to demineralisation progression
384 parallel along prismatic enamel (continuous permeation along rods or inter-rods). In addition,
385 the reason for the non-x-axis intercept at pH 5.5 for width was due to the acid exposure area
386 (hole in the varnish). This was because as soon as a pH initiated enamel demineralisation the
387 entire exposed surface area (width) would have started to become demineralised. The
388 phantom calibration curve was found to have a good fit with the power-law function to link
389 greyscale and mineral density ($y = ax^b$, $a = 18219.68$, $b = 0.66$, $R^2 = 0.996$) (Figure 7C).
390 Interestingly there was a linear relationship between mineral density and pH between pH 5.2-
391 4.0 with an x-axis intercept at ~ pH 5.5 ($y = y_0 + ax$, $y_0 = 12.44$, $a = -2.24$, $R^2 = 0.97$) (figure
392 7D) whereby there was no mineral density at the centre of the demineralised enamel at pH
393 4.0 and below. There appeared to be a correlation between complete mineral loss at the centre
394 of the lesions with a substantial increase in demineralised enamel area.

395

396

397

398

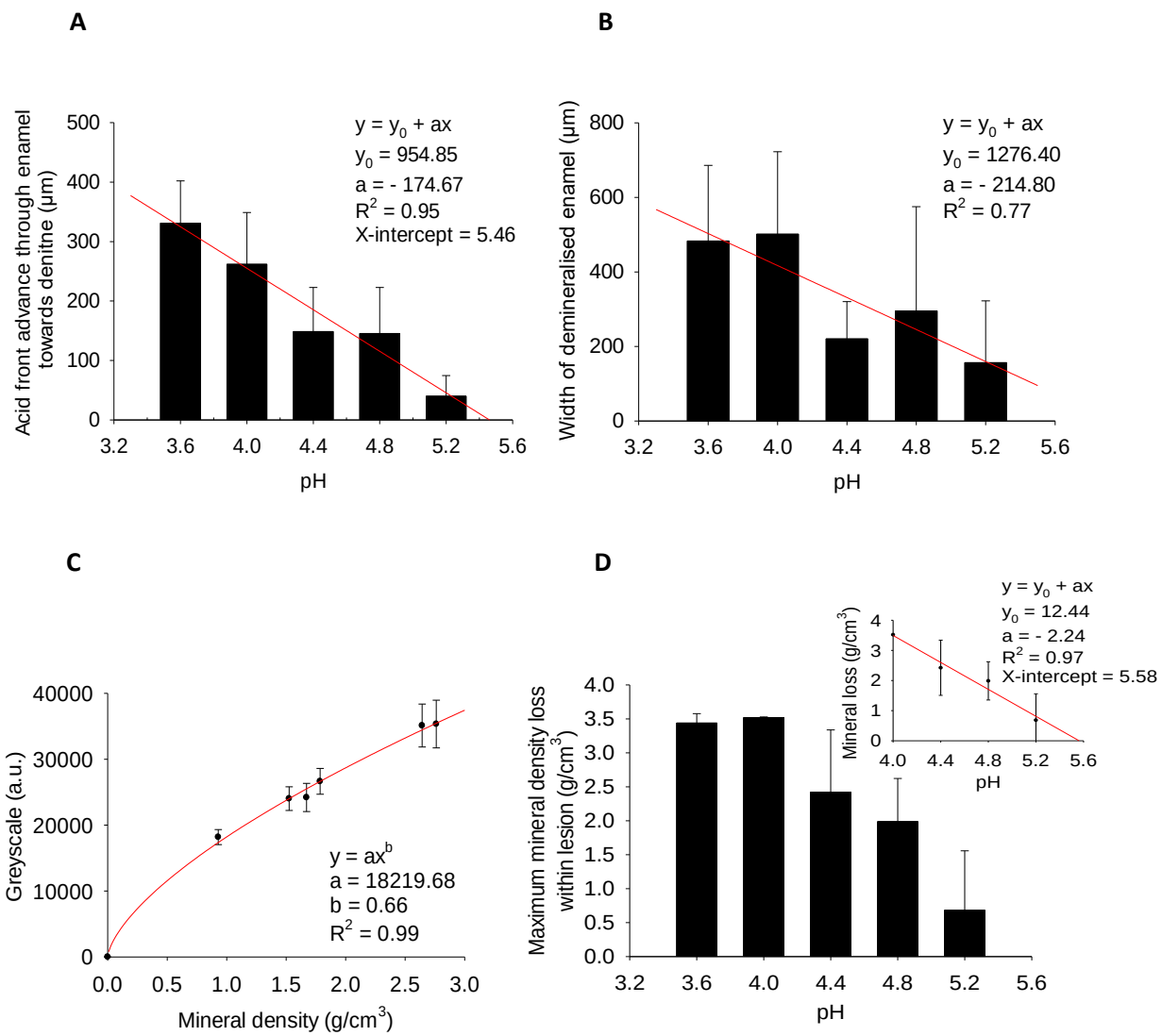

Figure 7: Dose-dependent response of lactic acid pH (0.5% v/v) with demineralised lesion depth (A), width (B) and maximum mineral density release (D). The plot D inset highlights a linear mineral release with pH acidity between ~ pH 5.5 (~ critical HAp pH/ x-axis intercept) and pH 4.0 (complete mineral loss). HAp phantom discs mineral density greyscale calibration (C). Data presented show mean ± standard deviation.

4. Discussion

Micro-CT equipment has been widely used to assess bone and dental tissue mineral density [27] and has been utilised by Davis et al to observe 3D *in situ* tooth demineralisation

[28]. The voxel size used by Davis et al [28] was 30 μm with a capture time of 2.6h, whereas in this study, micro-CT was used to capture *in situ* digital microradiographs (2D) at a pixel size of 3.02 μm with an ~1 minute capture time at each time point. This provided image resolution 10 times greater than Davis et al with more frequent time points. This allowed the accurate detection of the schmelzmuster mineral loss dynamics and enhanced correlation with PTLM. The data showed that lactic acid almost instantly induced disruption of the enamel surface and a continuous acid exposure resulted in preferential demineralisation of the sub-surface enamel, as previously observed in dental caries [29]. This advanced the work of Klinger & Wiedemann [20] and Davis et al [28], which generated enamel erosion data (complete surface mineral loss causing enamel thinning) possibly due to the use of a larger enamel exposure area to the acidic environment.

The surface zone feature of dental caries has been traditionally described [21]. It is thought to form due to a significant amount of fluorine (from toothpaste and mouthwashes) substituting hydroxyl groups in HAp crystallites producing fluorhydroxyapatite (FHAp) or fluorapatite (FAp) which occurs preferentially at the enamel free surface [30]. FAp has a lower average acid solubility than HAp, *i.e.* it has a critical pH of 4.5 compared with 5.5 for HAp [31] and consequently, regions of enamel with less FAp are more susceptible to acid dissolution. In addition to being chemically more resistant, the surface of enamel can be aprismatic in structure [32], and our data shows acid solubility of HAp is affected by crystallite orientation (Figure 4), therefore crystallite spatial arrangement can make the enamel surface physically (and naturally) more resistant to acids [17]. If the surface zone were only observed above the critical pH of FAp this would indicate only chemical resistance. However, a surface zone was observed also in lesions below the critical pH of FAp, which suggested that its existence did not depend exclusively on composition (FAp/FHAp ratios). Furthermore, the surface zone was not exclusively due to the existence of

aprismatic enamel as a surface zone was generated in enamel where the surface was partially ground. Therefore, the surface zone phenomena is at least partially influenced by another factor.

Sample 1 featured a lesion with a rounded demineralisation front at 85h whilst samples 2-4 had non-rounded fronts. This suggested that demineralisation progressed more isotropically in sample 1 and less so in samples 2-4. The reason for this variation between samples can again be explained by variations in HAp crystallite architecture (crystallite orientations that the acid meets) between samples. In the light microscopy experiments, these preferential demineralised front advances coincided with the HSBs. The HSBs are an optical effect caused by a change in the orientation of adjacent groups of enamel rods (and consequently crystallite orientation) [13]. The HSBs tend to be detectable in the inner two thirds of enamel, which may explain why the non-rounded shaped demineralisation front was observed several days into the experiments (once the acid had reached the HSBs). This is not the only place where preferential demineralisation takes place; it is well established that caries also spreads laterally when reaching the amelo-dentinal junction [33], however, the preferential demineralisation along the HSBs does not appear to have been reported before.

The demineralisation front advancement followed a power-law function (regardless of the shape of the lesion), this function had been hypothesised in a mathematical model of the progression of dental caries that our data and observations supported [34]. In addition, the minimum mineral density remaining in the lesions was found to follow an exponential decay model, which suggested preferential loss of a particular HAp orientation [8], [9] *i.e.* preferential enamel rod demineralisation leaving an intact inter-rod matrix behind as the acid front continued to advance. However, the total mineral loss was found to be linear over time hence the rate of lesion growth slowing and exponential decay model for minimum mineral density remaining were not due to diffusion inhibition of the mineral release over time but to

an increase in the acid front periphery area *i.e.* the number of rods in contact with the acid. In addition, the 21% higher demineralisation rate in depth over width again suggested that acid preferentially progressed along the enamel rods rather than across them. Also, whilst the total mineral release over time demonstrated a linear relationship it was noted that there appeared to be an initial lag period which could have been related to the generation of the surface zone *i.e.* the presence of FHAp/ FAp and aprismatic enamel. Alternatively, this could have been the observation of type 2 demineralisation transitioning to type 1 as seen in enamel caries [17].

Dental caries results in porosity detectable by micro-CT [28] as well as light microscopy [21]. However, our observations indicated that light refraction identified earlier changes in porosity than radiolucency changes detected by standard X-rays or even more sensitive micro-CT equipment. It might therefore be feasible to develop sensitive light-based caries detection systems rather than radiology based techniques. One issue with light-based diagnostics is the need for transmission through the tooth. While this was possible for 500 μm slices, it is more difficult to achieve when imaging whole teeth. Nevertheless, new non-ionising light based diagnostic tools [35] such as optical coherence tomography (OCT) are potentially clinically promising for early stage surface softening detection [36] but the penetration limitation does not allow high-resolution bulk enamel demineralisation imaging.

Published micro-CT data [37] shows that healthy enamel has a typical mineral density range between 2.65 – 2.89 g/cm^3 and can be as high as 3.2 g/cm^3 [38]. The top mineral density (2.76 g/cm^3) of the phantom within this work was therefore within the required range for healthy enamel mineral density. However, beam hardening at the edge of some tooth samples induced an artificially high mineral density at some enamel surfaces resulting in all the calibration bars being extrapolated beyond 3.2 g/cm^3 in figure 6 (note that images were still not saturated in those areas). This did not mean the surface zones observed were artefacts

as the surface zones were thinner than the beam hardening areas. In order to overcome the beam hardening issue the control mineral density was calculated below the beam hardening area of the samples and produced a mineral density value of 3.51 ± 0.46 g/cm^3 which was slightly above the previously published mineral density range but was considered acceptable for trend analysis with pH. Enamel carious lesions in the literature have reportedly reduced HAp mineral densities between 1.48 – 2.03 g/cm^3 (losing between 0.62 – 1.41 g/cm^3) compared with the surface zone retaining mineral density between 2.23 – 2.58 g/cm^3 (losing between 0.31 – 0.66 g/cm^3) [38]. This showed that the loss of mineral density in this work was more severe than occurs in natural carious lesions at every pH except the control.

However, the linear release of enamel mineral density with increasing pH acidity indicated a logarithmic relationship between mineral loss and proton concentration (due to the logarithmic nature of pH units). This suggested that enamel HAp crystallite orientation has a logarithmic relationship with acid solubility. The intercept of the linear mineral release trend at ~ pH 5.5 supported the linear model because this is near the critical pH of enamel. Previous literature showed that the rate of mineral release over time at different pH values was linear and that the pH affected the gradient of the mineral release linear equations [39] but our work showed that differences in pH environment also had a linear relationship with mineral release.

5. Conclusions

The present study quantified human enamel demineralisation dynamics using an acid-only caries model as a function of time and pH which revealed the total mineral loss with time was linear, whilst the minimum mineral density remaining within demineralised areas demonstrated exponential decay. This showed that a type of mineral environment within prismatic enamel structure *i.e.* rod or inter-rod was preferentially demineralised at a constant

519 rate. Comparison of X-rays with PTLM elucidated the importance of schmelzmuster level
520 HAp crystallite orientation (HSBs) in enamel demineralisation progression and showed light
521 detection is more sensitive to enamel demineralisation than X-rays. The linear rate of mineral
522 loss within the demineralised areas as a function of pH elucidates the relationship between
523 HAp orientation and acid solubility. *In vivo* it is likely that in a severely demineralised
524 enamel, the remaining prismatic scaffold might be susceptible to destruction by masticatory
525 forces, but nonetheless opens the possibility for developing effective therapeutic
526 remineralisation regimes at early stages of demineralisation.

527 **Acknowledgments**

528 This project was funded by EPSRC RCUK (EP/P005381/1) "Tackling human dental
529 caries by multi-modal correlative microscopy and multi-physics modelling".

530 **References**

[1] D. Ozdemir, Dental Caries: The most common disease worldwide and preventive strategies, Int. J. Biol. 5(4) (2013) 44-61, DOI: 10.5539/ijb.v5n4p55.

[2] A. BaniHani, C. Deery, J. Toumba, T. Munyombwe, M. Duggal, The impact of dental caries and its treatment by conventional or biological approaches on the oral health-related quality of life of children and carers, Int. J. Paediatr. Dent. 28(2) (2018) 266-276, DOI: 10.1111/ipd.12350.

[3] K.J. Chun, J.Y. Lee, Comparative study of mechanical properties of dental restorative materials and dental hard tissues in compressive loads, J. Dent. Biomech. 5: 1758736014555246 (2014).

[4] C. Sicca, E. Bobbio, N. Quartuccio, G. Nicolò, A. Cistaro, Prevention of dental caries: A review of effective treatments, J. Clin. Exp. Dent. 8(5) (2016) e604–e610.

[5] J.D.B. Featherstone, H. Rosenberg, Lipid effect on the progress of artificial carious lesions in dental enamel, Caries Res. 18 (1984) 52–55.

[6] R.M. Frank, Structural events in the caries process in enamel, cementum, and dentin, J. Dent. Res. 69(2_suppl) (1990) 559-566.

[7] R.P. Shellis, Relationship between human enamel structure and the formation of caries-like lesions in vitro, Arch. Oral Biol. 29(12) (1984) 975-981.

[8] R. Fabregas, J.A. Rubinstein, Mathematical model for the progression of dental caries, Math. Med. Biol. 31 (2014) 319–337.

[9] R. Fabregas, J. Rubinstein, On the initial propagation of dental caries, J. R. Soc. Interface. 11(100) (2014) 20140809.

[10] C. Xu, R. Reed, J.P. Gorski, Y. Wang, M.P. Walker, The distribution of carbonate in enamel and its correlation with structure and mechanical properties, J. Mater. Sci. 47(23) (2012) 8035–8043.

[11] C. Dawes, What is the critical pH and why does a tooth dissolve in acid?, J. Can. Dent. Assoc. 69(11) (2003) 722–4.

[12] R. Cheng, H. Yang, M. Shao, T. Hu, X. Zhou, Dental erosion and severe tooth decay related to soft drinks: a case report and literature review, J. Zhejiang Univ. Sci. B. 10(5) (2009) 395–399.

[13] A. Nanci, Ten Cate's oral histology development, structure and function, Sixth edition. St Louis, USA, 2003: Mosby, Inc; ISBN: 0-323-01614-6.

[14] L. Wang, R. Tang, T. Bonstein, C.A. Orme, P.J. Bush, G.H. Nancollas, A new model for nanoscale enamel dissolution, J. Phys. Chem. B. 109 (2005) 999-1005.

[15] L.M. Silverstone, C.A. Saxton, I.L. Dogon, O. Fejerskov, Variation in the pattern of acid etching of human dental enamel examined by scanning electron microscopy, Caries Res. 9 (1975) 373-387.

[16] T, Sui, E. Salvati, R.A. Harper, H. Zhang, R.M. Shelton, G. Landini, A.M. Korsunsky, *In situ* monitoring and analysis of enamel demineralisation using synchrotron X-ray scattering, Acta. Biomater. 77 (2018) 333-341.

[17] E.I.F. Pearce, D.G.A. Nelson, Microstructural features of carious human enamel imaged with back-scattered electrons, J. Dent. Res. 68(2) (1989) 113-118.

[18] E.D. Yilmaz, G.A. Schneider, M.V. Swain, Influence of structural hierarchy on the fracture behaviour of tooth enamel, Phil. Trans. R. Soc. A. 373 (2015) 20140130.

[19] C. E. Smith, Y. Hu, J. C-C. Hu, J. P. Simmer, Characteristics of the transverse 2D uniserial arrangement of rows of decussating enamel rods in the inner enamel layer of mouse mandibular incisors, J. Anat. 235 (2019) 912—930.

[20] H.G. Klinger, W. Wiedemann, A method for radiographic longitudinal study of mineral content during *in-vitro* demineralisation and remineralisation of human tooth enamel, Arch. Oral Biol. 30 (1985) 373-375.

[21] C. Robinson, R.C. Shore, S.J. Brookes, S. Strafford, S.R. Wood, J. Kirkham, The chemistry of enamel caries, Crit. Rev. Oral Biol. Med. 11(4) (2000) 481-49.

[22] E.A.A. Neel, A. Aljabo, A. Strange, S. Ibrahim, M. Coathup, A.M. Young, L. Bozec, V, Mudera, Demineralization–remineralization dynamics in teeth and bone, Int. J. Nanomedicine. 11 (2016) 4743–4763.

[23] H.C. Margolis, E.C. Moreno, Composition and cariogenic potential of dental plaque fluid, Crit. Rev. Oral Biol. Med. 5(1) (1994) 1-25.

[24] A.C.B. Delbem, A.E.M. Vieira, K.T. Sassaki, M.L. Cannon, S.R. Stock, X. Xiao, F. DeCarlo, Quantitative analysis of mineral content in enamel using synchrotron microtomography and microhardness analysis, Proc. SPIE 6318, Developments in X-Ray Tomography V. 631824 (2006).

[25] K.U. Barthel, (barthel at htw-berlin.de), Internationale Medieninformatik, HTW Berlin, Berlin, Germany. Available at: https://imagej.nih.gov/ij/plugins/volume-viewer.html [accessed 28th September 2018].

[26] B. Lee, P. Chou, S. Chen, H. Liao, C. Chang, Prevention of enamel demineralization with a novel fluoride strip: enamel surface composition and depth profile, Sci. Rep. 5 (2015) 13352.

[27] C.H. Park, Z.R. Abramson, M. Taba Jr, Q. Jin, J. Chang, J.M. Kreider, S.A. Goldstein, W.V. Giannobile, Three-dimensional micro-computed tomographic imaging of alveolar bone in experimental bone loss or repair, J. Periodontol. 78(2) (2007) 273–281.

[28] G. R. Davis, D Mills, P. Anderson, Real-time observations of tooth demineralization in 3 dimensions using X-ray microtomography, J. Dent. 69 (2018) 88-92.

[29] L.M. Silverstone, Surface phenomena in dental caries, Nature. 214 (1967) 203–204.

[30] O.Y. Yu, M.L. Mei, I.S. Zhao, E.C.M. Lo, C.H. Chu, Effects of fluoride on two chemical models of enamel demineralization, Materials. 10 (2017) 1245.

[31] J.H. Meurman, J.M. ten Cate, Pathogenesis and modifying factors of dental erosion, Eur. J. Oral Sci. 104 (1996) 199-206.

[32] D.K. Whittaker, Structural variations in the surface zone of human tooth enamel observed by scanning electron microscopy, Arch. Oral Biol. 27(5) (1982) 383-392.

[33] K.R. Ekstrand, D.N. Ricketts, E.A. Kidd, Do occlusal carious lesions spread laterally at the enamel-dentin junction? A histolopathological study, Clin. Oral Investig. (1) (1998) 15-20.

[34] R. Fabregas, PhD thesis, Universidad Complutense de Madrid. A mathematical model for the progression of dental caries, 2014.

[35] J. Gomez, Detection and diagnosis of the early caries lesion, BMC Oral Health. 15(Suppl 1) (2015) S3.

[36] A. Aden, P. Anderson, G. R. Burnett, R. J. M. Lynch, P. H. Tomlins, Longitudinal correlation of 3D OCT to detect early stage erosion in bovine enamel, Biomed. Opt. Express. 8 (2017) 954-973.

[37] T.T. Huang, A.S. Jones, L.H. He, M.A. Darendeliler, M.V. Swain, Characterisation of enamel white spot lesions using X-ray micro-tomography, J. Dent. 35(9) (2007) 737-43.

[38] S.E.P Dowker, J.C. Elliott, G.R. Davis, H.S. Wassif, Longitudinal study of the three-dimensional development of subsurface enamel lesions during in vitro demineralisation, Caries Res. 37 (2003) 237–245.

[39] H.C. Margolis, Y.P. Zhang, C.Y. Lee, R.L. Kent, E.C. Moreno, Kinetics of enamel demineralization in vitro, J. Dent. Res. 78(7) (1999) 1326-1335.